

pubs.acs.org/acscatalysis Research Article

# Intrinsic Catalytic Activity of Carbon Nanotubes for Electrochemical Nitrate Reduction

Nia J. Harmon, <sup>⊥</sup> Conor L. Rooney, <sup>⊥</sup> Zixu Tao, Bo Shang, Neera Raychaudhuri, Chungseok Choi, Huaping Li, and Hailiang Wang\*



Cite This: ACS Catal. 2022, 12, 9135-9142



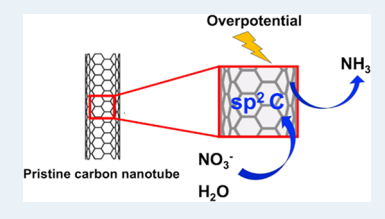
**ACCESS** I

III Metrics & More

Article Recommendations

SI Supporting Information

**ABSTRACT:** We study a variety of carbon nanotubes (CNTs) as cost-effective catalysts for the electrochemical nitrate (NO $_3$ <sup>-</sup>) reduction reaction, which holds promise for converting environmental NO $_3$ <sup>-</sup> pollutants into useful ammonia (NH $_3$ ) products. We discover that pristine multi-walled carbon nanotubes (MWCNTs) exhibit notable electrocatalytic activity for NO $_3$ <sup>-</sup> reduction to NH $_3$  in a near-neutral electrolyte. Single-walled carbon nanotubes have even higher activity and selectivity than MWCNTs for this reaction. Results from control experiments confirm that this activity originates from the native carbon surface rather than from metal impurities. Contrary to the prevalent notion that heteroatom doping into carbon materials



increases their electrocatalytic performance, we find that introducing oxygen and nitrogen functional groups into MWCNTs reduces their electrocatalytic activity for  $NO_3^-$  reduction. After analyzing the potential-dependent electrocatalytic performance of the CNT catalysts, we further report an interesting positive correlation between total current density and Faradaic efficiency for  $NH_3$  formation irrespective of the type of CNT. This correlation suggests deeper  $NO_3^-$  reduction at higher reaction rates regardless of the catalyst identity. The findings presented in this work suggest a unique type of active site for electrocatalytic  $NO_3^-$  reduction, therefore broadening the role of carbon materials in electrocatalysis.

KEYWORDS: electrocatalysis, nitrate reduction, carbon nanotubes, ammonia synthesis, water treatment

## INTRODUCTION

Fertilizer runoff from agricultural activity is a major source of nitrate (NO<sub>3</sub><sup>-</sup>) contamination in groundwater and surface water. The uncontrolled release of NO<sub>3</sub><sup>-</sup> into watersheds poses a serious threat to human health and the environment. In humans, infant methemoglobinemia, a potentially fatal blood disorder, and cancer can result from ingesting NO<sub>3</sub><sup>-.2-4</sup> In view of the health concerns associated with NO<sub>3</sub><sup>-</sup> pollution, the World Health Organization recommends a maximum  $NO_3^-$  concentration of 50 mg  $L^{-1}$  in drinking water.<sup>2,4</sup>  $NO_3^$ pollution also has negative environmental consequences because it contributes to eutrophication and damages local ecosystems.<sup>5</sup> To remove NO<sub>3</sub><sup>-</sup> from water, various methods have been used including ion exchange, reverse osmosis, and bacterial denitrification, but these processes also produce waste brine or sludge that requires expensive treatment or disposal.5-8 The electrochemical NO<sub>3</sub>- reduction reaction (NO<sub>3</sub>RR) is an alternative strategy that can transform NO<sub>3</sub> into products such as harmless N2, valuable ammonia (NH3), or several others, including NO, NO<sub>2</sub><sup>-</sup>, N<sub>2</sub>O, and NH<sub>2</sub>OH. <sup>9–18</sup> NO<sub>3</sub>RR is attracting increasing attention because of its potential advantages over traditional water treatment processes, most notably, the opportunity to capture and recycle waste NO<sub>3</sub><sup>-</sup> into NH<sub>3</sub> using renewable electricity. Additionally, NO<sub>3</sub>RR could provide a sustainable alternative to the fossilfuel-reliant Haber-Bosch process for the synthesis of NH3, a

product widely used as a fertilizer, chemical feedstock, and fuel.  $^{5,19}$ 

As a result, there is increasing interest in developing active and selective electrocatalysts for converting NO<sub>3</sub><sup>-</sup> to NH<sub>3</sub>. To date, NO<sub>3</sub>RR studies have utilized a diverse assortment of catalysts including metals, 13,20-22 metal oxides, 9,23 bimetallic systems, 24-26 and single-metal atoms embedded in doped carbon materials.<sup>27,28</sup> While carbon nanomaterials are used as metal-free electrocatalysts in a range of reactions, including the oxygen reduction reaction, <sup>29–32</sup> hydrogen evolution reaction, <sup>33</sup> oxygen evolution reaction,<sup>34</sup> and organic transformation reactions, 35,36 there are only a few reports of their use in NO<sub>3</sub>RR. These limited examples include defective graphene,<sup>3</sup> nitrogen-doped graphene, 38 and fluorine-doped carbon synthesized from the carbonization of a polytetrafluoro-ethylene-saturated cigarette filter.<sup>39</sup> Their electrocatalytic activity is associated with defects or heteroatom dopants. Given the wide application of carbon nanomaterials, including carbon nanotubes (CNTs), in catalysis, 40-42 it is desirable to further explore their potential as cheap and abundant

Received: March 6, 2022 Revised: June 25, 2022



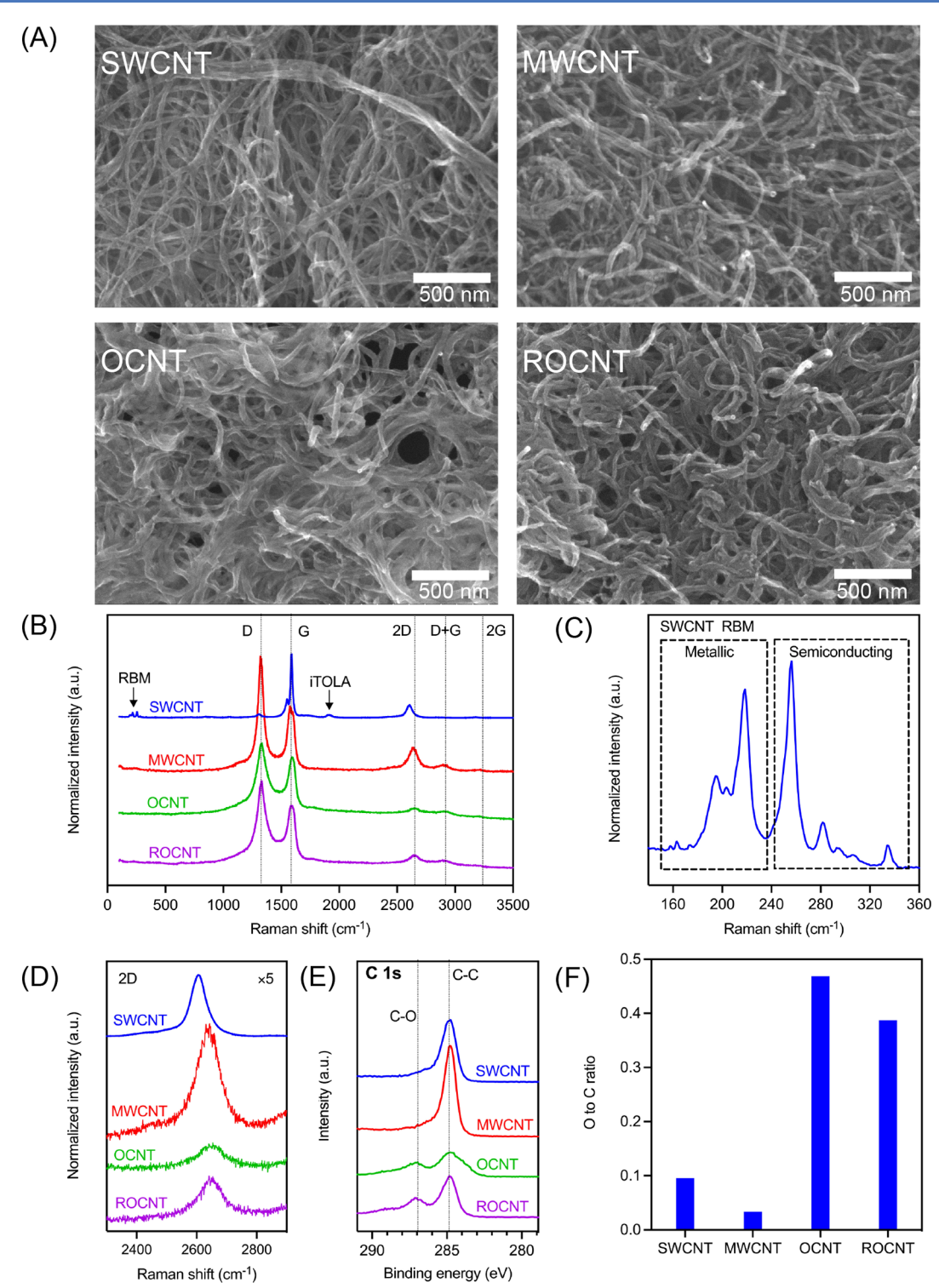


Figure 1. Structural characterization of CNTs. (A) SEM images. (B) Raman spectra. All spectra were normalized to the intensity of the G band. (C) Enlarged RBM region of SWCNTs. (D) 2D bands with 5× magnification. (E) C 1s XPS spectra. (F) Atomic O/C ratios measured by XPS.

electrocatalysts for NO<sub>3</sub>RR. It is also interesting to answer the fundamental question of whether pristine carbon surfaces can catalyze the reaction.

In this work, we studied various CNTs for NO<sub>3</sub><sup>-</sup> electroreduction, including multi-walled carbon nanotubes (MWCNTs), single-walled carbon nanotubes (SWCNTs), mildly oxidized MWCNTs (OCNTs), and reduced OCNTs (ROCNTs). We discovered that MWCNTs, without metal impurities, have intrinsic activity for NO<sub>3</sub>RR. In a near-neutral

electrolyte containing 0.4 M KNO $_3$ , MWCNTs achieve a Faradaic efficiency (FE) toward NH $_3$  of 73% and an average current density of 25 mA cm $^{-2}$  at -0.85 V vs the reversible hydrogen electrode (RHE; all potentials in this work are referenced to the RHE scale unless otherwise noted). Notably, after introducing heteroatoms (O and N) into the MWCNT structure, the resulting OCNTs and N-doped carbon nanotubes (NCNTs) show much lower activity and selectivity for NO $_3$ <sup>-</sup> reduction to NH $_3$ . Our findings challenge the prevalent

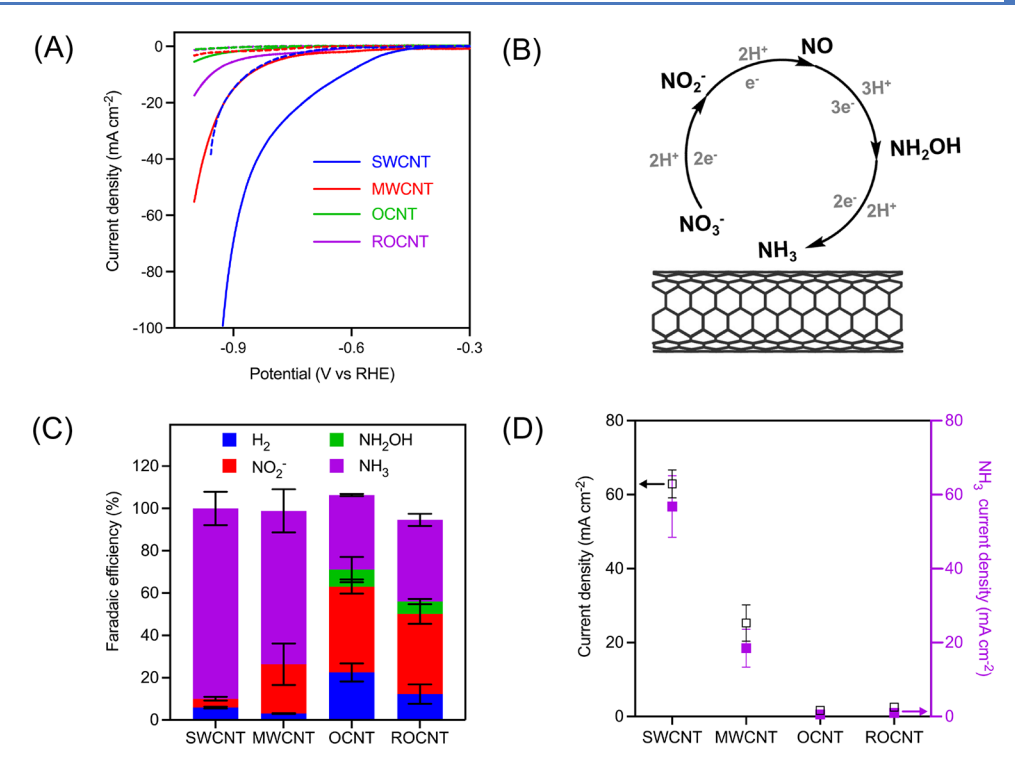


Figure 2.  $NO_3^-$  reduction catalysis of CNTs. (A) LSVs recorded at a scan rate of 5 mV s<sup>-1</sup> in Ar-saturated 0.1 M PB + 0.4 M KNO<sub>3</sub> (solid line) vs 0.1 M PB (dashed line). (B) Possible reaction pathway of  $NO_3^-$  reduction to  $NH_3$ . (C) Product distribution and (D) current density for different CNTs at -0.85 V in 0.1 M PB + 0.4 M KNO<sub>3</sub>. The error bars represent the standard deviations of multiple measurements. Note that there are error bars for OCNT and ROCNT, but they do not appear because they are shorter than the size of the symbol.

notion that heteroatom doping into carbon-based nanomaterials improves their electrocatalytic activity. We also found that SWCNT surfaces are substantially more active and selective for NH $_3$  production than MWCNT surfaces. Elemental analysis of SWCNTs reveals that they still contain Fe from their synthesis even after purification. However, we confirmed that Fe is not exposed on the surface and, thus, most of the observed catalytic performance likely originates from the SWCNT surface. We also evaluated the effect of the applied potential on the activity and selectivity of the CNTs toward NO $_3^-$  reduction to NH $_3$ . Our results indicate a general positive correlation between total current density and FE (NH $_3$ ) irrespective of the catalyst identity. Taken together, these findings suggest a new type of reactivity originating from pristine carbon surfaces.

# ■ RESULTS AND DISCUSSION

In order to prepare and characterize the catalyst materials, we started by purifying as-received MWCNTs via calcination and acid treatment as detailed in our previous work.<sup>43</sup> To prepare OCNTs, we oxidized purified MWCNTs using a modified Hummers method, 44 which were then thermally treated in an Ar atmosphere to create ROCNTs. We purified as-obtained SWCNTs by heating them in an aqueous mixture of H<sub>2</sub>O<sub>2</sub> and HCl.45 Additional experimental details are available in the Supporting Information (SI). To understand the structures of the different CNTs, we characterized their morphology, extent of graphitization, and surface composition. We observed the morphology and microstructure of SWCNTs, MWCNTs, OCNTs, and ROCNTs using scanning electron microscopy (SEM) (Figure 1A). SWCNTs, with an average diameter of  $\sim$ 1 nm, are bundled in powder form. MWCNTs appear less aggregated, with entangled individual tubes that are micrometers long and  $\sim$ 20 nm in diameter. SEM images reveal that the oxidation or further reduction of MWCNTs does not alter their morphology.

To characterize the structures and defect levels of the CNTs, we employed Raman spectroscopy. The Raman spectra of CNTs have three main characteristic bands (Figure 1B): the D band (~1350 cm<sup>-1</sup>) represents the contribution of disorder or defects, the G band (~1580 cm<sup>-1</sup>) originates from the stretching of the C-C bonds within the graphitic structure, and the 2D band (also called the G' band,  $\sim 2600 \text{ cm}^{-1}$ ) is the D band overtone that appears in graphitic materials. 46-54 The SWCNT material exhibits a strong G band and a very weak D band, indicating a high-quality graphitic structure. Both the radial breathing mode (RBM) (~100-400 cm<sup>-1</sup>) and the high-frequency iTOLA combination mode (~1915 cm<sup>-1</sup>), which are unique to SWCNTs, are observed. 46-54 The RBM features reveal that the SWCNTs are a mixture of metallic and semiconducting tubes (Figure 1C). Pristine MWCNTs show a much more prominent D band than SWCNTs, indicating a higher defect level. Upon oxidation of MWCNTs, the resulting OCNTs display a lower D to G band ratio  $(I_D/I_G)$ , broader D and G bands, and a weaker 2D band (Figure 1B,D and Table S1). These features are associated with the introduction of functional groups and defects by oxidation. 55,56 Reduction of OCNTs to ROCNTs increases the  $I_D/I_G$  ratio (Table S1) and the intensity of the 2D band. This indicates that partial restoration of the graphitic structure occurs during the reduction process.57

Considering that electrocatalysis predominantly takes place on the catalyst surface, we used X-ray photoelectron spectroscopy (XPS) to study the surface chemical structures of the different CNTs (Figure 1E and Figure S1). Both SWCNTs and MWCNTs show a single C 1s peak centered at

284.8 eV, which corresponds to sp<sup>2</sup>-hybridized C. 55,58 For OCNTs and ROCNTs, a second peak appears at a higher binding energy of ~287 eV and can be assigned to functional groups containing O bonded to C atoms. 53,58 In general, an increase in the width of the peak centered at 284.8 eV signals an increase in disorder or non-uniformity in the CNT material. 55,58-60 The presence of a peak at ~287 eV and broadening of the peak located at 284.8 eV are spectral features consistent with the introduction of functional groups and defects by oxidation. 55,58 Reduction of OCNTs to produce ROCNTs decreases the relative intensity of the C-O peak and the width of the C-C peak, suggesting that the process does repair OCNTs to some degree but is unable to fully restore the original MWCNT structure. XPS elemental analysis reveals low O/C ratios for MWCNT and SWCNT surfaces (Figure 1F). Consistent with the C 1s spectra, there is a substantial amount of oxygen in the surface layers of OCNTs and ROCNTs with a slight decrease in the O/C ratio after the reduction process.

After characterizing the CNTs, we sought to assess their electrocatalytic activity using a two-compartment H-cell with Ar-saturated aqueous electrolyte containing 0.1 M phosphate buffer (PB, pH = 7.2) + 0.4 M KNO<sub>3</sub>. The linear sweep voltammograms (LSVs) are plotted in Figure 2A. Comparing them with their corresponding LSVs measured in the same PB electrolyte without NO<sub>3</sub><sup>-</sup> reveals the onset potentials for NO<sub>3</sub>RR (Figure S2). Notably, OCNTs show substantially lower catalytic activity than pristine MWCNTs: the onset potential is shifted more negatively by 450 mV, and the current is smaller at all scanned potentials. ROCNTs are more active than OCNTs but are still considerably less active than MWCNTs. These results indicate that the oxygen functional groups and defects on the surface of the OCNTs and, to a lesser extent, the ROCNTs suppress the intrinsic activity of the graphitic MWCNT surface. Interestingly, SWCNTs are even more active than MWCNTs: the onset potential is 10 mV more positive, and the current density reaches 100 mA cm<sup>-2</sup> at -0.93 V.

We also studied the catalytic selectivity of the different CNT materials. According to the literature, the likely reaction pathway for NO<sub>3</sub>RR in aqueous electrolyte is shown in Figure 2B.9-18 Some possible intermediates formed along the eightelectron reduction pathway from NO<sub>3</sub><sup>-</sup> to NH<sub>3</sub> include NO<sub>2</sub><sup>-</sup>, NO, and NH2OH. To determine product selectivity, we performed controlled potential electrolysis (CPE) measurements at a cathodic potential of -0.85 V. Gas (H<sub>2</sub>)- and liquid (NO<sub>2</sub><sup>-</sup>, NH<sub>2</sub>OH, and NH<sub>3</sub>)-phase products were quantified by gas chromatography and colorimetric methods, respectively (Figure S3). Other possible gaseous products such as NO, N<sub>2</sub>O<sub>2</sub>, and N<sub>2</sub> are not detected. The CPE results show that SWCNTs catalyze NO<sub>3</sub><sup>-</sup> reduction to NH<sub>3</sub> with the highest NH<sub>3</sub> FE of 90% and a total current density of 63 mA cm<sup>-2</sup> (Figure 2C,D). Other detected products are  $NO_2^-$  (FE = 4%) and H<sub>2</sub> (FE = 6%). MWCNTs deliver a NH<sub>3</sub> FE of 73%, a NO<sub>2</sub><sup>-</sup> FE of 23%, and a total current density of 25 mA cm<sup>-2</sup>. OCNTs are the least selective and active toward NH3 with a FE of 35% and a total current density of 1.6 mA cm<sup>-2</sup>; NO<sub>2</sub> becomes a major product (FE = 41%), and NH<sub>2</sub>OH is also formed. When compared to OCNTs, ROCNTs show a marginally higher NH<sub>3</sub> selectivity (FE = 39%) and total current density (2.5 mA cm<sup>-2</sup>).

The rate and selectivity for NO<sub>3</sub>RR of all of the CNT electrocatalysts can be tuned via the applied potential. The

potential dependence of product selectivity and total current density for the SWCNT, MWCNT, OCNT, and ROCNT materials are plotted in Figure S4. All of the CNT materials follow a general trend in which NH<sub>3</sub> production is enhanced at more negative potentials. Interestingly, we observe a positive correlation between FE (NH<sub>3</sub>) and total current density when we plot all of the data points from the different CNTs together (Figure 3). Within the applied potential range considered in

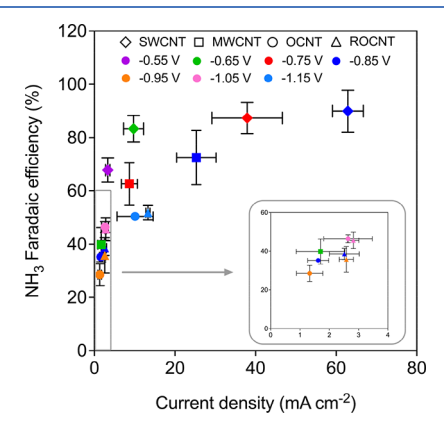


Figure 3. Current density influences  $NH_3$  production on different CNT surfaces. Correlation between  $NH_3$  FE and current density. The error bars represent the standard deviations of multiple measurements. Note that some error bars do not appear because they are shorter than the size of the symbol. The inset is a zoomed-in view of the lower current density region.

this study, we observe that FE (NH<sub>3</sub>) generally increases with  $j_{\text{total}}$  in the relatively low reaction rate region ( $j_{\text{total}} < 4$  mA cm<sup>-2</sup>). As the current density increases further, FE (NH<sub>3</sub>) gradually converges toward a maximum value. This relationship suggests that larger current densities appear to favor the complete reduction of NO<sub>3</sub><sup>-</sup> to NH<sub>3</sub> on graphitic carbon surfaces.

The electrocatalytic results indicate that pristine CNT surfaces are active for NO<sub>3</sub>RR and that oxygen doping diminishes catalytic activity. These findings challenge the conventional understanding that the introduction of heteroatoms into a sp<sup>2</sup> C structure modulates the electronic structure and consequently enhances the activity for electrocatalytic reactions. <sup>31,61</sup> To further investigate this phenomenon, we also considered if a similar reduction in catalytic activity could be observed in NCNTs (Figure S5). Control experiments with NCNTs (Figures S6 and S7) show that they have a lower catalytic performance than pristine MWCNTs. When compared to MWCNTs, NCNTs show a lower NH3 selectivity (FE = 53%) and total current density (15 mA cm<sup>-2</sup>) at -0.85V. Therefore, we can confirm that doping MWCNTs with O and N functional groups does reduce the NO<sub>3</sub>RR performance of the sp<sup>2</sup> C surface, albeit the reduction in performance is not the same across all CNTs. A possible explanation for this phenomenon is that the C atoms on the CNT surface are active sites, whereas the electron-rich O or N functional groups simply reduce the number of active sites or may even hamper effective adsorption of the negatively charged NO<sub>3</sub><sup>-</sup> reactant via electrostatic repulsion. For example, our zeta potential measurements reveal negative charges on the surface of OCNTs at near-neutral pH, which are not present on the MWCNT surface (Figure S8). These negative surface charges, which are likely caused by carboxylic acid groups formed in the

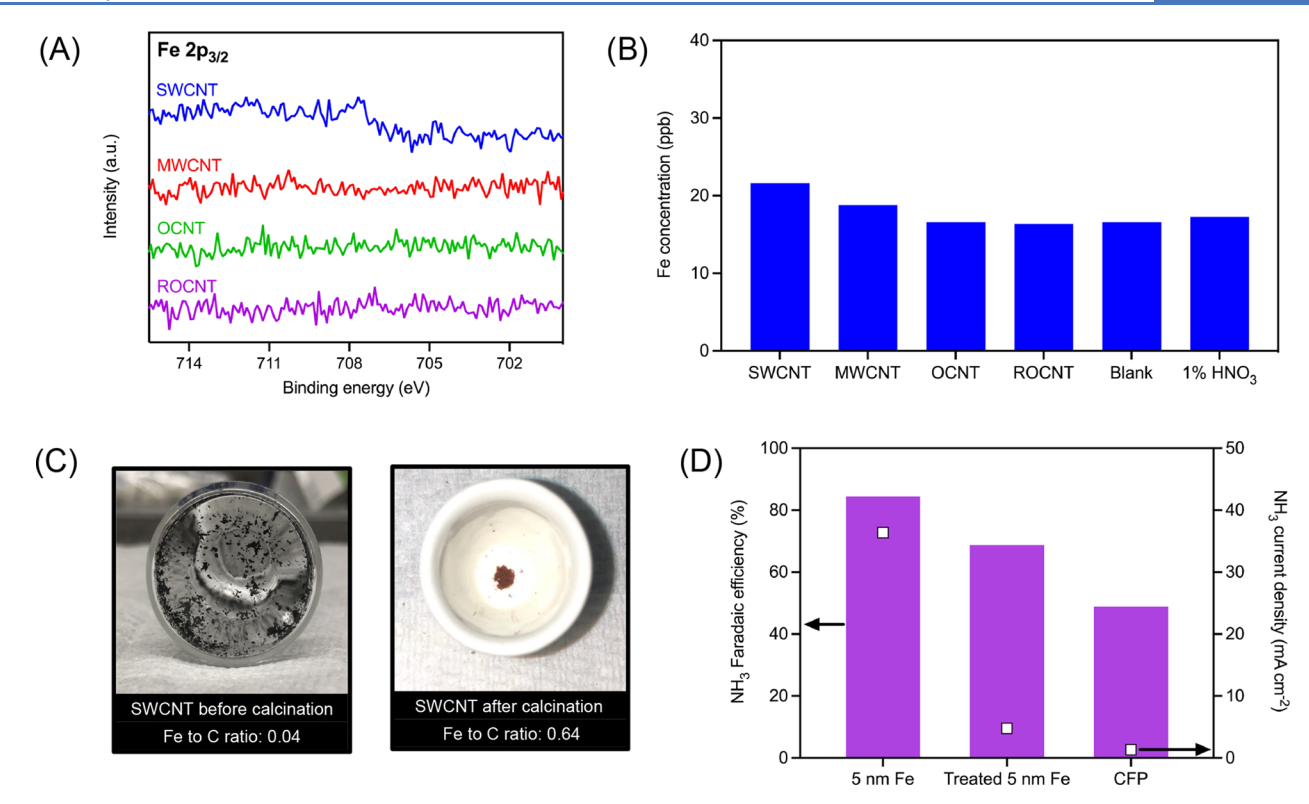


Figure 4. Evidence of Fe contamination in SWCNTs and  $NO_3^-$  reduction performance of Fe-coated electrodes. (A) Fe  $2p_{3/2}$  XPS spectra of CNTs. (B) ICP-MS elemental analysis of Fe in CNTs, a blank sample, and 1% HNO<sub>3</sub>. (C) Photographs of SWCNTs before and after calcination. (D) Activity of CFP coated with 5 nm of Fe and after treating the electrode with HCl and  $H_2O_2$ . Results are from a 30 min CPE at -0.80 V in Arsaturated 0.1 M PB + 0.4 M KNO<sub>3</sub>.

CNT oxidation process,  $^{56,62}$  may repel NO<sub>3</sub><sup>-</sup> from approaching the catalyst surface. Our hypothesis that C is the true active site for NO<sub>3</sub>RR on the CNT electrocatalysts can also explain the unified FE (NH<sub>3</sub>)- $j_{\text{total}}$  relationship (Figure 3) since all of the materials possess these active sites.

Of the two best-performing CNT materials, we found that SWCNTs are considerably more active than MWCNTs. One possibility is that the SWCNT material has a much higher surface area due to the much smaller diameter of SWCNTs compared to MWCNTs. This possibility is eliminated, however, by our measurements of the electrochemically active surface area (ECSA) using the electrochemical double layer capacitance technique (see the SI for details; Figure S9). We show that the SWCNT material has an even smaller ECSA than MWCNTs. Alternatively, C atoms on the SWCNT surface may be intrinsically more active than those on the MWCNT surface. The larger curvature of SWCNTs, which alters the bonding geometry and, consequently, the electronic structure of the C atoms, may be a contributor. This hypothesis will be tested in future work.

Since both the MWCNTs and SWCNTs used in this study were synthesized using metal (Fe) catalysts, <sup>63,64</sup> it is necessary to verify that the observed electrocatalytic reactivities are not caused by catalyst residues. First, we checked the four CNT materials using XPS. The results show no prominent Fe signals (Figure 4A), suggesting that the CNT surfaces do not contain Fe. This is a reasonable result if we consider the strong acid treatment employed in our purification processes, which should remove all exposed Fe species. We then examined the bulk material via inductively coupled plasma mass spectrometry (ICP-MS). The samples were prepared by calcining the CNTs and then digesting the ash with HNO<sub>3</sub>. Essentially no

Fe is found in MWCNTs, OCNTs, or ROCNTs (Figure 4B). No other metal impurities are detected in the CNTs (Table S2). While the ICP-MS sample of SWCNTs also shows an Fe concentration comparable to the background level (Figure 4B), we note that the ash contains reddish-brown powder that is not fully digested by HNO<sub>3</sub> (Figure 4C). Energy dispersive X-ray spectroscopy (EDS) analysis of the ash reveals that it contains a significant amount of Fe (Figure 4C and Figure S10). The fact that these Fe species can survive strong acid digestion indicates that they are likely encapsulated rather than exposed on the surface, which is consistent with the XPS results. To further verify that the Fe impurities in SWCNTs are not exposed and thus do not directly contribute to NO<sub>3</sub>RR catalytic activity, we performed a control experiment with 5 nm of Fe deposited on a carbon fiber paper (CFP) electrode substrate. While metallic Fe is considerably active for NO<sub>3</sub><sup>-</sup> reduction to NH<sub>3</sub>, treatment with HCl and H<sub>2</sub>O<sub>2</sub> (the same condition used in the SWCNT purification procedure) eliminates most of the activity, approaching the background level of a bare CFP electrode (Figure 4D and Figure S11). We also performed XPS analysis on a SWCNT electrode after a 1 h CPE measurement at -0.85 V in 0.1 M PB + 0.4 M KNO<sub>3</sub> and confirmed that no Fe residues migrate to the surface of the SWCNT electrode under electrochemical conditions (Figure S12). Therefore, it is reasonable to conclude that the NO<sub>3</sub>RR active sites on SWCNTs are C-based. Finally, we checked the electrolyte solutions and the MWCNT electrode before and after electrolysis to verify that no metal contamination is introduced by the electrolyte or during the electrolysis (Table S3).

ACS Catalysis pubs.acs.org/acscatalysis Research Article

#### CONCLUSIONS

In summary, we have demonstrated that pristine CNTs (both MWCNTs and SWCNTs) are active and selective electrocatalysts for the reduction of NO<sub>3</sub><sup>-</sup> to NH<sub>3</sub>. Heteroatom doping decreases the catalytic performance and indicates that C is the active site for NO<sub>3</sub>RR. We find a positive correlation between NH<sub>3</sub> production and total current density regardless of the type of CNT surface. The results presented here provide evidence for a new type of active site for NO<sub>3</sub>RR, which may benefit future catalyst design. Future work will focus on investigating the reaction mechanism and the NO<sub>3</sub>RR performance of CNTs using concentrations of nitrate typically found in contaminated groundwater.

## ASSOCIATED CONTENT

# **3** Supporting Information

The Supporting Information is available free of charge at https://pubs.acs.org/doi/10.1021/acscatal.2c01144.

Experimental details, additional material characterization, and electrochemical and ICP-MS results (PDF)

## AUTHOR INFORMATION

# **Corresponding Author**

Hailiang Wang — Department of Chemistry, Yale University, New Haven, Connecticut 06520, United States; Energy Sciences Institute, Yale University, West Haven, Connecticut 06516, United States; orcid.org/0000-0003-4409-2034; Email: hailiang.wang@yale.edu

#### Authors

- Nia J. Harmon Department of Chemistry, Yale University, New Haven, Connecticut 06520, United States; Energy Sciences Institute, Yale University, West Haven, Connecticut 06516, United States
- Conor L. Rooney Department of Chemistry, Yale University, New Haven, Connecticut 06520, United States; Energy Sciences Institute, Yale University, West Haven, Connecticut 06516, United States; orcid.org/0000-0001-7058-568X
- Zixu Tao Department of Chemistry, Yale University, New Haven, Connecticut 06520, United States; Energy Sciences Institute, Yale University, West Haven, Connecticut 06516, United States; orcid.org/0000-0002-6670-1796
- Bo Shang Department of Chemistry, Yale University, New Haven, Connecticut 06520, United States; Energy Sciences Institute, Yale University, West Haven, Connecticut 06516, United States
- Neera Raychaudhuri Department of Chemical and Environmental Engineering, Yale University, New Haven, Connecticut 06520, United States
- Chungseok Choi Department of Chemistry, Yale University, New Haven, Connecticut 06520, United States; Energy Sciences Institute, Yale University, West Haven, Connecticut 06516, United States
- **Huaping Li** Chemelectronics LLC, Inglewood, California 90301, United States

Complete contact information is available at: https://pubs.acs.org/10.1021/acscatal.2c01144

# **Author Contributions**

<sup>1</sup>N.J.H. and C.L.R. contributed equally to this work.

#### **Notes**

The authors declare no competing financial interest.

#### ACKNOWLEDGMENTS

This work was supported by the U.S. National Science Foundation (grant CBET2028351). N.J.H. acknowledges the Ford Foundation Predoctoral Fellowship.

## REFERENCES

- (1) Galloway, J. N.; Townsend, A. R.; Erisman, J. W.; Bekunda, M.; Cai, Z.; Freney, J. R.; Sutton, M. A. Transformation of the Nitrogen Cycle. *Science* **2008**, *320*, 889–892.
- (2) Ward, M. H.; deKok, T. M.; Levallois, P.; Brender, J.; Gulis, G.; Nolan, B. T.; VanDerslice, J. Workgroup report: Drinking-water nitrate and health Recent findings and research needs. *Environ. Health Perspect.* **2005**, *113*, 1607–1614.
- (3) Follett, R. F.; Hatfield, J. L. Nitrogen in the environment: sources, problems, and management. Sci. World J. 2001, 1, 920–926.
- (4) Duca, M.; Koper, M. T. M. Powering denitrification: The perspectives of electrocatalytic nitrate reduction. *Energy Environ. Sci.* **2012**, *5*, 9726–9742.
- (5) Wang, Z.; Richards, D.; Singh, N. Recent discoveries in the reaction mechanism of heterogeneous electrocatalytic nitrate reduction. *Catal. Sci. Technol.* **2021**, *11*, 705–725.
- (6) Rezvani, F.; Sarrafzadeh, M. H.; Ebrahimi, S.; Oh, H. M. Nitrate removal from drinking water with a focus on biological methods: a review. *Environ. Sci. Pollut. Res.* **2019**, *26*, 1124–1141.
- (7) Zeng, Y.; Priest, C.; Wang, G.; Wu, G. Restoring the Nitrogen Cycle by Electrochemical Reduction of Nitrate: Progress and Prospects. *Small Methods* **2020**, **December 1**, *4*, 2000672.
- (8) Barrabés, N.; Sá, J. Catalytic nitrate removal from water, past, present and future perspectives. *Appl. Catal., B* **2011, April 27**, *104*, 1–5.
- (9) Jia, R.; Wang, Y.; Wang, C.; Ling, Y.; Yu, Y.; Zhang, B. Boosting Selective Nitrate Electroreduction to Ammonium by Constructing Oxygen Vacancies in TiO2. ACS Catal. 2020, 10, 3533–3540.
- (10) Taguchi, S.; Feliu, J. M. Kinetic study of nitrate reduction on Pt(1 1 0) electrode in perchloric acid solution. *Electrochim. Acta* **2008**, 53, 3626–3634.
- (11) Li, J.; Zhan, G.; Yang, J.; Quan, F.; Mao, C.; Liu, Y.; Yu, J. C. Efficient Ammonia Electrosynthesis from Nitrate on Strained Ruthenium Nanoclusters. J. Am. Chem. Soc. 2020, 142, 7036–7046.
- (12) Kuwabata, S.; Uezumi, S.; Tanaka, K.; Tanaka, T. Assimilatory and Dissimilatory Reduction of NO3- and NO2- with an (n-Bu4N)3[Mo2Fe6S8(SPh)9] Modified Glassy-Carbon Electrode in Water. *Inorg. Chem.* **1986**, 25, 3018–3022.
- (13) Pérez-Gallent, E.; Figueiredo, M. C.; Katsounaros, I.; Koper, M. T. M. Electrocatalytic reduction of Nitrate on Copper single crystals in acidic and alkaline solutions. *Electrochim. Acta* **2017**, 227, 77–84.
- (14) Petrii, O. A.; Akbaeva, Y. A.; Safonova, T. Y.; Kondrasheva, V. S.; Kolosov, E. N.; Tsirlina, G. A.; Gryaznov, V. M. Intensification of the nitrate anion reduction on a membrane palladium electrode. *Russ. J. Electrochem.* **2002**, *38*, 220–223.
- (15) Yao, Y.; Zhu, S.; Wang, H.; Li, H.; Shao, M. A Spectroscopic Study of Electrochemical Nitrogen and Nitrate Reduction on Rhodium Surfaces. *Angew. Chem.* **2020**, *59*, 10479–10483.
- (16) Katsounaros, I.; Kyriacou, G. Influence of nitrate concentration on its electrochemical reduction on tin cathode: Identification of reaction intermediates. *Electrochim. Acta* **2008**, *53*, 5477–5484.
- (17) De Vooys, A. C. A.; Beltramo, G. L.; Van Riet, B.; Van Veen, J. A. R.; Koper, M. T. M. Mechanisms of electrochemical reduction and oxidation of nitric oxide. In *Electrochimica Acta* 2004, 49, 1307–1314. DOI: 10.1016/j.electacta.2003.07.020
- (18) Lacasa, E.; Cañizares, P.; Llanos, J.; Rodrigo, M. A. Removal of nitrates by electrolysis in non-chloride media: Effect of the anode material. *Sep. Purif. Technol.* **2011**, *80*, 592–599.

- (19) van Langevelde, P. H.; Katsounaros, I.; Koper, M. T. M. Electrocatalytic Nitrate Reduction for Sustainable Ammonia Production. *Joule* **2021**, *5*, 290–294.
- (20) Fu, X.; Zhao, X.; Hu, X.; He, K.; Yu, Y.; Li, T.; Kang, Y. Alternative route for electrochemical ammonia synthesis by reduction of nitrate on copper nanosheets. *Appl. Mater. Today* **2020**, *19*, 100620.
- (21) Huang, C. P.; Wang, H. W.; Chiu, P. C. Nitrate reduction by metallic iron. *Water Res.* 1998, 32, 2257–2264.
- (22) Lim, J.; Liu, C. Y.; Park, J.; Liu, Y. H.; Senftle, T. P.; Lee, S. W.; Hatzell, M. C. Structure Sensitivity of Pd Facets for Enhanced Electrochemical Nitrate Reduction to Ammonia. *ACS Catal.* **2021**, *11*, 7568–7577
- (23) Wang, Y.; Zhou, W.; Jia, R.; Yu, Y.; Zhang, B. Unveiling the Activity Origin of a Copper-based Electrocatalyst for Selective Nitrate Reduction to Ammonia. *Am. Ethnol.* **2020**, *132*, 5388–5392.
- (24) Wang, Y.; Xu, A.; Wang, Z.; Huang, L.; Li, J.; Li, F.; Sargent, E. H. Enhanced Nitrate-to-Ammonia Activity on Copper-Nickel Alloys via Tuning of Intermediate Adsorption. *J. Am. Chem. Soc.* **2020**, *142*, 5702–5708.
- (25) Wang, Z.; Young, S. D.; Goldsmith, B. R.; Singh, N. Increasing electrocatalytic nitrate reduction activity by controlling adsorption through PtRu alloying. *J. Catal.* **2021**, *395*, 143–154.
- (26) Hamid, S.; Bae, S.; Lee, W.; Amin, M. T.; Alazba, A. A. Catalytic Nitrate Removal in Continuous Bimetallic Cu-Pd/Nanoscale Zerovalent Iron System. *Ind. Eng. Chem. Res.* **2015**, *54*, 6247–6257.
- (27) Wu, Z. Y.; Karamad, M.; Yong, X.; Huang, Q.; Cullen, D. A.; Zhu, P.; Wang, H. Electrochemical ammonia synthesis via nitrate reduction on Fe single atom catalyst. *Nat. Commun.* **2021**, *12*, 2870.
- (28) Lei, F.; Xu, W.; Yu, J.; Li, K.; Xie, J.; Hao, P.; Tang, B. Electrochemical synthesis of ammonia by nitrate reduction on indium incorporated in sulfur doped graphene. *Chem. Eng. J.* **2021**, 426, 131317.
- (29) Xu, X.; Jiang, S.; Hu, Z.; Liu, S. Nitrogen-doped carbon nanotubes: High electrocatalytic activity toward the oxidation of hydrogen peroxide and its application for biosensing. *ACS Nano* **2010**, *4*, 4292–4298.
- (30) Gong, K.; Du, F.; Xia, Z.; Durstock, M.; Dai, L. Nitrogen-doped carbon nanotube arrays with high electrocatalytic activity for oxygen reduction. *Science* **2009**, 323, 760–764.
- (31) Rocha, I. M.; Soares, O. S. G. P.; Figueiredo, J. L.; Freire, C.; Pereira, M. F. R. Bifunctionality of the pyrone functional group in oxidized carbon nanotubes towards oxygen reduction reaction. *Catal. Sci. Technol.* **2017**, *7*, 1868–1879.
- (32) Qu, L.; Liu, Y.; Baek, J. B.; Dai, L. Nitrogen-doped graphene as efficient metal-free electrocatalyst for oxygen reduction in fuel cells. *ACS Nano* **2010**, *4*, 1321–1326.
- (33) Zheng, Y.; Jiao, Y.; Zhu, Y.; Li, L. H.; Han, Y.; Chen, Y.; Qiao, S. Z. Hydrogen evolution by a metal-free electrocatalyst. *Nat. Commun.* **2014**, *5*, 3783.
- (34) Zhao, Y.; Nakamura, R.; Kamiya, K.; Nakanishi, S.; Hashimoto, K. Nitrogen-doped carbon nanomaterials as non-metal electrocatalysts for water oxidation. *Nat. Commun.* **2013**, *4*, 2390.
- (35) Xie, X.; Long, J.; Xu, J.; Chen, L.; Wang, Y.; Zhang, Z.; Wang, X. Nitrogen-doped graphene stabilized gold nanoparticles for aerobic selective oxidation of benzylic alcohols. *RSC Adv.* **2012**, *2*, 12438–12446.
- (36) Yang, H.; Cui, X.; Dai, X.; Deng, Y.; Shi, F. Carbon-catalysed reductive hydrogen atom transfer reactions. *Nat. Commun.* **2015**, *6*, 6478.
- (37) Kamiya, K.; Hashimoto, K.; Nakanishi, S. Graphene Defects as Active Catalytic Sites that are Superior to Platinum Catalysts in Electrochemical Nitrate Reduction. *ChemElectroChem* **2014**, *1*, 858–862
- (38) Zhao, J.; Shang, B.; Zhai, J. N-doped graphene as an efficient metal-free electrocatalyst for indirect nitrate reduction reaction. *Nanomaterials* **2021**, *11*, 2418.

- (39) Li, Y.; Xiao, S.; Li, X.; Chang, C.; Xie, M.; Xu, J.; Yang, Z. A robust metal-free electrocatalyst for nitrate reduction reaction to synthesize ammonia. *Materials Today Physics* **2021**, *19*, 100431.
- (40) Planeix, J. M.; Coustel, N.; Coq, B.; Brotons, V.; Kumbhar, P. S.; Dutartre, R.; Geneste, P.; Bernier, P.; Ajayan, P. M. Application of Carbon Nanotubes as Supports in Heterogeneous Catalysis. *J. Am. Chem. Soc.* **1994**, *116*, 7935–7936.
- (41) Yan, Y.; Miao, J.; Yang, Z.; Xiao, F. X.; Yang, H. B.; Liu, B.; Yang, Y. Carbon nanotube catalysts: Recent advances in synthesis, characterization and applications. *Chem. Soc. Rev.* **2015**, *44*, 3295–3346
- (42) Rodríguez-Reinoso, F. The role of carbon materials in heterogeneous catalysis. *Carbon* **1998**, *36*, 159–175.
- (43) Wu, Y.; Jiang, Z.; Lu, X.; Liang, Y.; Wang, H. Domino electroreduction of CO2 to methanol on a molecular catalyst. *Nature* **2019**, *575*, 639–642.
- (44) Hummers, W. S.; Offeman, R. E. Preparation of Graphitic Oxide. J. Am. Chem. Soc. 1958, 80, 1339.
- (45) Wang, Y.; Shan, H.; Hauge, R. H.; Pasquali, M.; Smalley, R. E. A highly selective, one-pot purification method for single-walled carbon nanotubes. *J. Phys. Chem. B* **2007**, *111*, 1249–1252.
- (46) Dresselhaus, M. S.; Dresselhaus, G.; Saito, R.; Jorio, A. Raman spectroscopy of carbon nanotubes. *Phys. Rep.* **2005**, **March**, *409*, 47–99.
- (47) Dresselhaus, M. S.; Jorio, A.; Hofmann, M.; Dresselhaus, G.; Saito, R. Perspectives on carbon nanotubes and graphene Raman spectroscopy. *Nano Lett.* **2010**, *10*, 751–758.
- (48) Wu, J. B.; Lin, M. L.; Cong, X.; Liu, H. N.; Tan, P. H. Raman spectroscopy of graphene-based materials and its applications in related devices. *Chem. Soc. Rev.* **2018**, *47*, 1822–1873.
- (49) Ferrari, A. C.; Meyer, J. C.; Scardaci, V.; Casiraghi, C.; Lazzeri, M.; Mauri, F.; Geim, A. K. Raman spectrum of graphene and graphene layers. *Phys. Rev. Lett.* **2006**, *97*, 187401.
- (50) Ferrari, A. C.; Basko, D. M. Raman spectroscopy as a versatile tool for studying the properties of graphene. *Nat. Nanotechnol.* **2013**, *8*, 235–246.
- (51) Gupta, R.; Singh, B. P.; Singh, V. N.; Gupta, T. K.; Mathur, R. B. Origin of radial breathing mode in multiwall carbon nanotubes synthesized by catalytic chemical vapor deposition. *Carbon* **2014**, *66*, 724–726.
- (52) Lehman, J. H.; Terrones, M.; Mansfield, E.; Hurst, K. E.; Meunier, V. Evaluating the characteristics of multiwall carbon nanotubes. *Carbon* **2011**, 2581–2602.
- (53) Kuzmany, H.; Plank, W.; Hulman, M.; Kramberger, C.; Gr, A. Determination of SWCNT diameters from the Raman response. *Eur. Phys. J. B* **2001**, 22, 307–320.
- (54) Tian, Y.; Jiang, H.; Laiho, P.; Kauppinen, E. I. Validity of Measuring Metallic and Semiconducting Single-Walled Carbon Nanotube Fractions by Quantitative Raman Spectroscopy. *Anal. Chem.* **2018**, *90*, 2517–2525.
- (55) Datsyuk, V.; Kalyva, M.; Papagelis, K.; Parthenios, J.; Tasis, D.; Siokou, A.; Galiotis, C. Chemical oxidation of multiwalled carbon nanotubes. *Carbon* **2008**, *46*, 833–840.
- (56) Vanyorek, L.; Meszaros, R.; Barany, S. Surface and electrosurface characterization of surface-oxidized multi-walled N-doped carbon nanotubes. *Colloids Surf., A* **2014**, *448*, 140–146.
- (57) Wang, H.; Robinson, J. T.; Li, X.; Dai, H. Solvothermal reduction of chemically exfoliated graphene sheets. *J. Am. Chem. Soc.* **2009**, *131*, 9910–9911.
- (58) Okpalugo, T. I. T.; Papakonstantinou, P.; Murphy, H.; McLaughlin, J.; Brown, N. M. D. High resolution XPS characterization of chemical functionalised MWCNTs and SWCNTs. *Carbon* **2005**, *43*, 153–161.
- (59) Duan, J.; Chen, S.; Jaroniec, M.; Qiao, S. Z. Heteroatom-Doped Graphene-Based Materials for Energy-Relevant Electrocatalytic Processes. ACS Catal. 2015, 5, 5207–5234.
- (60) Wang, H.; Maiyalagan, T.; Wang, X. Review on recent progress in nitrogen-doped graphene: Synthesis, characterization, and its potential applications. *ACS Catal.* **2012**, *2*, 781–794.

- (61) Li, J. C.; Hou, P. X.; Liu, C. Heteroatom-Doped Carbon Nanotube and Graphene-Based Electrocatalysts for Oxygen Reduction Reaction. *Small* **2017**, *13*, 1702002.
- (62) Jiang, L.; Gao, L. Carbon nanotubes-metal nitride composites: A new class of nanocomposites with enhanced electrical properties. *J. Mater. Chem.* **2005**, *15*, 260–266.
- (63) Smits, J.; Wincheski, B.; Namkung, M.; Crooks, R.; Louie, R. Response of Fe powder, purified and as-produced HiPco single-walled carbon nanotubes to flash exposure. *Mater. Sci. Eng., A* **2003**, 358, 384–389.
- (64) Wei, F.; Zhang, Q.; Qian, W. Z.; Yu, H.; Wang, Y.; Luo, G. H.; Wang, D. Z. The mass production of carbon nanotubes using a nanoagglomerate fluidized bed reactor: A multiscale space-time analysis. *Powder Technol.* **2008**, *183*, 10–20.